

Creating lattice gauge potentials in circuit QED: The bosonic Creutz ladderHadiseh Alaeian,¹ Chung Wai Sandbo Chang,² Mehran Vahdani Moghaddam,² Christopher M. Wilson,² Enrique Solano,^{3,4,5} and Enrique Rico^{3,4}¹*Physikalisches Institut, Universitat Stuttgart, Pfaffenwaldring 57, 70569 Stuttgart, Germany*²*IQC and Electrical and Computer Engineering department, University of Waterloo, 200 University Ave. West Waterloo, Ontario, Canada N2L 3G1*³*Department of Physical Chemistry, University of the Basque Country UPV/EHU, Apartado 644, 48080 Bilbao, Spain*⁴*IKERBASQUE, Basque Foundation for Science, Maria Diaz de Haro 3, E-48013 Bilbao, Spain*⁵*Department of Physics, Shanghai University, 200444 Shanghai, China*

(Received 28 January 2019; published 22 May 2019)

In this work we propose two protocols to make an effective gauge potential for microwave photons in circuit QED. The first scheme is based on coupled transmons whose on-site energies are harmonically modulated in time. We investigate the effect of various types of capacitive and inductive couplings, and the role of the phase difference between adjacent sites on creating a complex hopping rate between coupled qubits. The second method relies on the parametrically coupling the modes of a SQUID in a resonator and controlling the hopping phase via a coherent pump. Both proposals can be readily realized in a superconducting circuit with the existing technology and are suitable for scalable lattices. As an example benefiting from these complex-valued hopping terms, we simulated the behavior of a plaquette of bosonic Creutz ladder as one of the important models with interdisciplinary interest in various branches of physics. Our results clearly show the emergence of chiral edge modes and directional transport between lattice sites. Combined with intrinsic nonlinearity of the transmon qubits such lattices would be an ideal platform for simulating many different Hamiltonians such as the Bose–Hubbard model with nontrivial gauge fields. Important direct applications of the presented results span a broad range from signal processing in nonreciprocal transport to quantum simulation of gauge-invariant models in fundamental physics.

DOI: [10.1103/PhysRevA.99.053834](https://doi.org/10.1103/PhysRevA.99.053834)**I. INTRODUCTION**

Coherence and coherent effects are the hallmarks of quantum systems. The flourishing and growing field of circuit quantum electrodynamics (circuit QED) in recent years have opened a horizon in quantum control and coherent studies via benefiting from the quantized electromagnetic fields of a circuit, mimicking an atom with discrete states. The controllability and ease of tunability of circuit QED elements make them powerful candidates for some of the large-scale, integrated quantum networks. So far, circuit QED is almost the only engineerable quantum system. Its properties arise from the quantized electric charge and magnetic flux making a harmonic ladder. Besides, the Josephson junction is the main nonlinear element leading to an anharmonic ladder with unequal energy spacing to realize an artificial atom.

In circuit QED, the atom-light interactions are implemented via a combination of the microwave resonators and superconducting qubits on an integrated chip with diverse experimental control [1]. The system can easily be extended to large-scale lattices for realizing efficient simulators for Bose–Hubbard, and Jaynes–Cummings–Hubbard models. Moreover, due to the inherent openness of the system, circuit QED provides a unique platform to investigate driven-dissipative systems and study the strong correlations and nonequilibrium physics [2–8]. Another unique feature of circuit QED is the possibility of studying quantum phenomena on macroscopic scales. Benefiting from the inherent nonlinearity of

the Josephson junction an interaction between superconductor qubits can be realized, as well.

Photons are the best information carriers due to their ease of control, accessibility, and preparation. Moreover, the recent advancements in the realm of photonics have made it possible to manipulate and steer them almost arbitrarily. Therefore, for making a large-scale network of qubits, photons are one of the obvious choices. However, photons are neutral particles without any charge, so they do not lend themselves to magnetic-field manipulations, trivially. Recently an artificial gauge field has been synthesized from the atom-light interaction that controls the flow of the neutral photons as if they are charged particles and move in a magnetic field [9,10].

In this article we report on the control of dynamical coupling between two superconducting qubits in a microwave circuit. We employ light-matter coupling to induce photon-photon interactions and generate an effective magnetic field for the photons. By periodically modulating the energy of a Josephson junction in a transmon qubit, or by controlling the coupling between the modes of a SQUID in a resonator, we show the emergence of an effective magnetic field as a nontrivial phase in the hopping term between adjacent nodes [11–13]. In contrast to other systems, the parameters of this setup, such as on-site energy, interaction between the adjacent sites, and the driving frequency, can be varied over a wide range. The effect of this phase on the photon transport is studied in a lattice of coupled bosonic nodes arranged in a plaquette, where a directional photon transport along the

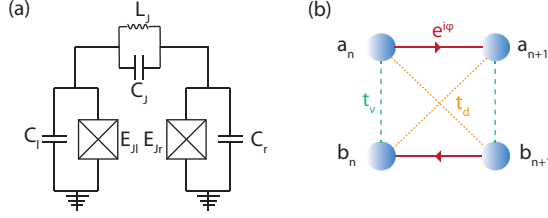


FIG. 1. (a) A circuit of two transmons coupled with both inductive and capacitive elements. (b) Schematics of a plaquette from a bosonic Creutz ladder showing all the nodes and the coupling terms.

plaquette edge has been demonstrated. This topological feature can be further utilized to make a protected photon transport in a disordered lattice as previously proposed and demonstrated in other coupled-resonator systems [14,15].

This work is organized as follows: In the second section we derive the effective Hamiltonian of two coupled transmon qubits whose Josephson junction's energies are harmonically modulated in time. We show how this modulation generates a complex hence, nonreciprocal hopping between coupled qubits. Moreover, we propose another scheme based on SQUIDs for making a complex hopping between cavity modes that is realizable with the existing circuit QED technology. In the third section we study the effect of this complex coupling term in a bosonic Creutz ladder, an important model appearing in different disciplines of physics. There, we briefly introduce the model and derive its symmetries and the chiral properties arising from a nonreciprocal coupling. For the sake of brevity we focus on one plaquette of the Creutz ladder, where we explicitly show how some of the nontrivial features of the ladder, including the chiral modes and edge states, are achievable in this plaquette. Finally, section four concludes the paper and presents some of the immediate theoretical and experimental follow-up works. The study and the results of this paper present a road map for simulating important Hamiltonians such as bosonic Creutz ladder and Bose-Hubbard lattice with circuit QEDs.

II. NONRECIPROCAL COUPLING VIA PARAMETRIC MODULATION

A. On-site energy modulation of transmons in an array

Transmon qubits are some of the important building blocks of circuit QED. A brief review on some of their basic important properties and a list of relevant references can be found in Appendix A. The system of our interest is composed of two transmons coupled together via a capacitor or an inductor as shown in Fig. 1(a). Moreover, the energy of the Josephson junction of each transmon is assumed to be periodically modulated in time. The effect of modulation in creating nontrivial gauge fields has been investigated for about a decade in different realms of physics [16–18] and very recently in circuit QED [19]. In this section we are interested in investigating those effects in a circuit QED lattice composed of coupled transmons. As elaborated in Appendix B in detail, this problem can be transformed to a more general problem of two coupled bosonic degrees of freedom whose on-site energies are time-harmonically modulated. The nodes are

coupled together via a particle-conserving operator described with an effective hopping term from one node to the other. In this section we employ the Floquet theorem to investigate the effect of this modulation on the general behavior of the system.

Although the calculations and results are presented for a two-site lattice only, the same treatment is applicable to an extended lattice with many nodes. The interested reader may refer to relevant references for further information and elaboration on the Floquet theorem [20–22].

As derived in Eq. (B7), the Hamiltonian of two bosonic nodes with time-harmonically modulated energies and a fixed coupling rate J is given as

$$\begin{aligned} \hat{H}(t)/\hbar = & -J(\hat{a}_2^\dagger \hat{a}_1 + \hat{a}_1^\dagger \hat{a}_2) \\ & + [\omega_{01} + \Omega_{01} \cos(\omega_M t + \phi_1)] \left(\hat{a}_1^\dagger \hat{a}_1 + \frac{1}{2} \right) \\ & + [\omega_{02} + \Omega_{02} \cos(\omega_M t + \phi_2)] \left(\hat{a}_2^\dagger \hat{a}_2 + \frac{1}{2} \right). \end{aligned} \quad (1)$$

For every node described as a harmonic oscillator, Fock space is the eigenspace of the number operator and satisfies the following relation

$$\omega_m \left(\hat{a}_m^\dagger \hat{a}_m + \frac{1}{2} \right) |n\rangle_m = \omega_m \left(n_m + \frac{1}{2} \right) |n\rangle_m, \quad (2)$$

where m is the lattice-site index.

Now consider that in Eq. (2) the trapping frequency is periodically modulated in time with frequency ω_M as $\omega_m = \omega_{0m} + \Omega_{0m} \cos(\omega_M t + \phi_m)$. For this modified harmonic oscillator we define the following rotated Fock states:

$$\begin{aligned} |N\rangle_m = & |n\rangle_m \exp[-i\omega_{0m}(n_m + 1/2)t] \exp \\ & \times \left[-i \frac{\Omega_{0m}}{\omega_M} (n_m + 1/2) \sin(\omega_M t + \phi_m) \right]. \end{aligned} \quad (3)$$

This state is composed of three main parts: (1) the Fock state, (2) a free-propagation of the Fock state given by the first exponential, and (3) a time-harmonically modulated rotation given by the second exponential. It is straightforward to show that this state is a solution of the periodically modulated harmonic oscillator Hamiltonian appearing in Eq. (1). In other words, the time-periodic modulation of the trap frequency changes the instantaneous frequency of each Fock state, and the new basis is related to the old ones via the following transformation:

$$\begin{aligned} R_m(t) = & \exp[-i\omega_{0m}(n_m + 1/2)t] \exp \\ & \times \left[-i \frac{\Omega_{0m}}{\omega_M} (n_m + 1/2) \sin(\omega_M t + \phi_m) \right]. \end{aligned} \quad (4)$$

In this rotated basis frame the transformed Hamiltonian reads

$$\hat{H}_{\text{rot}}(t) = \hat{U}^\dagger(t) \hat{H}(t) \hat{U}(t) - i\hbar \hat{U}^\dagger(t) \dot{\hat{U}}(t), \quad (5)$$

where $\hat{U}(t) = \otimes_m R_m(t)$ is the unitary transformation with $R_m(t)$ elements. The Hamiltonian of Eq. (1) in the rotated frame reads

$$\begin{aligned} \hat{H}_{\text{rot}}(t)/\hbar = & -J \exp \left(i \left[\frac{\Omega_{02}}{\omega_M} \sin(\omega_M t + \phi_2) - \frac{\Omega_{01}}{\omega_M} \right. \right. \\ & \left. \left. \times \sin(\omega_M t + \phi_1) \right] \right) e^{i(\omega_{02} - \omega_{01})t} \hat{a}_2^\dagger \hat{a}_1 + \text{H.c.} \end{aligned} \quad (6)$$

This form implies that the modulation of the on-site energy of each node with a fixed hopping rate to the adjacent node is equivalent to an effective modulation of the hopping rate.

For the sake of simplicity we assume that the modulation depth is the same for all nodes, i.e., $\Omega_{02} = \Omega_{01} = \Omega_0$. Knowing that $e^{ix \sin \theta} = \sum_{n=-\infty}^{\infty} \mathcal{J}_n(x) e^{in\theta}$, where $\mathcal{J}_n(x)$ is the n th-order Bessel function of first kind, the periodic Hamiltonian in Eq. (6) can be expressed in terms of partial Hamiltonians as¹

$$\begin{aligned} \hat{H}_{\text{rot}}(t)/\hbar &= -J e^{i(\omega_{02} - \omega_{01})t} \sum_{n=-\infty}^{+\infty} i^n e^{in \frac{\phi_1 + \phi_2}{2}} \\ &\times \mathcal{J}_n \left[\frac{2\Omega_0}{\omega_M} \sin \left(\frac{\phi_2 - \phi_1}{2} \right) \right] e^{in\omega_M t} \hat{a}_2^\dagger \hat{a}_1 + \text{H.c.} \end{aligned} \quad (7)$$

The n th partial Hamiltonian becomes stationary when $n\omega_M = \omega_{01} - \omega_{02}$. If the modulation frequency matches the energy difference between two adjacent sites (i.e., $\omega_M = \omega_{01} - \omega_{02}$) then the Hamiltonian in Eq. (6) would be simplified as

$$\hat{H}/\hbar = -iJ e^{i \frac{\phi_1 + \phi_2}{2}} \mathcal{J}_1 \left[\frac{2\Omega_0}{\omega_M} \sin \left(\frac{\phi_2 - \phi_1}{2} \right) \right] \hat{a}_2^\dagger \hat{a}_1 + \text{H.c.} \quad (8)$$

This final form indicates that the on-site energy modulation can be translated to a nontrivial change in the hopping rate between the coupled sites. Depending on the energy difference between the lattice sites and the modulation frequency, the effective coupling can be engineered to be a real number or a complex value. While the former corresponds to a reciprocal hopping between two sites the latter is an asymmetric coupling meaning that the i th \rightarrow j th coupling rate is not the same for the reverse direction.

For the sake of completeness, we study the effect of the different energy scales in the two-site problem where the initial Hamiltonian is given by $\hat{H}/\hbar = -J(\hat{a}_2^\dagger \hat{a}_1 + \hat{a}_1^\dagger \hat{a}_2) + [\frac{\omega}{2} + \Omega \sin(\omega t)](\hat{a}_1^\dagger \hat{a}_1 - \hat{a}_2^\dagger \hat{a}_2)$. Going to a rotated basis we get

$$\begin{aligned} \hat{H}_{\text{rot}}(t)/\hbar &= -J e^{-i[\omega t - \frac{2\Omega}{\omega} \cos(\omega t)]} \hat{a}_2^\dagger \hat{a}_1 + \text{H.c.} \\ &= -J \sum_m i^m \mathcal{J}_m \left(\frac{2\Omega}{\omega} \right) e^{i(m-1)\omega t} \hat{a}_2^\dagger \hat{a}_1 + \text{H.c.} \\ &\xrightarrow{\text{RWA}} -iJ \mathcal{J}_1 \left(\frac{2\Omega}{\omega} \right) \hat{a}_2^\dagger \hat{a}_1 + \text{H.c.} \end{aligned} \quad (9)$$

Figure 2 shows the occupation probability of the single-particle states at node 1 and 2 for different frequencies ω . As can be seen from Eq. (9), the full response consists of higher harmonics in the decomposition of the hopping term. Nonetheless, in the rotating wave approximation, i.e., when

¹Note that for $n = 0$ the coupling rate is still real, meaning a reciprocal coupling between adjacent sites. To break this symmetry one has to keep at least the first term in the expansion. Besides, it is not a stationary Hamiltonian. Moreover, note that the contribution of these higher-order terms vanish when the modulation vanishes, i.e., $\Omega_0 = 0$ as physically expected.

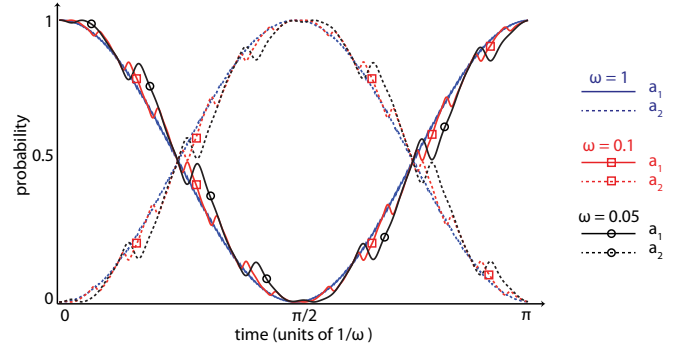


FIG. 2. Time evolution of a two-site problem with one excitation driven by a modulated onsite frequency with frequency ω and amplitude of the modulation Ω . $\omega = \Omega$ in all cases.

the energy scale of the modulating frequency ω is higher than the amplitude of the modulations, $\mathcal{J}_m(\frac{2\Omega}{\omega})$, just the nonoscillatory or stationary term will determine the whole dynamics. In these calculations, this condition is achieved by maximizing the value of the amplitude for the $m = 1$ mode with $\Omega \sim \omega$, such that all the others are much smaller. As can be seen in Fig. 2, the exact behavior deviates from the typical particle swap behavior further when the on-site and modulation frequency decreases. This is clear in the behavior of the red and black lines (lines with square and circular markers), dashed and solid, when the overall exchange behavior has some additional faster features compared with the blue lines. These features are due to the higher-energy terms contributed by higher harmonics.

Added as a new feature to the existing toolbox of circuit QED this nonreciprocal coupling can substantially extend the capability of this technology as a versatile quantum simulator beyond what has been achieved so far [23,24]. In the next section we study one of the important models that could be simulated with this added capability.

B. Parametric modulation of cavity modes

The modulating flux scheme proposed in the previous section is completely general and fully applicable for realizing the complex coupling required in the Creutz ladder. For a four-site plaquette however, we propose another scheme in this section that benefits from another commonly used circuit QED setup based on SQUIDS which is readily realizable [25–28]. The setup parametrically couples the total flux in a cavity, $\hat{\Phi}_c$, to the pump flux $\hat{\Phi}_p$ through a Hamiltonian as

$$\hat{H}_{SQ} = E_J |\cos(\pi \hat{\Phi}_p / \Phi_0)| \cos(2\pi \hat{\Phi}_c / \Phi_0). \quad (10)$$

The interaction Hamiltonian can be derived by expanding \hat{H}_{SQ} to the first order in $\hat{\Phi}_p$ around a flux bias Φ_{ext} , and to the second order in $\hat{\Phi}_c$ around zero. After applying the parametric approximation to the pump we get the following interaction Hamiltonian:

$$\hat{H}_{\text{int}} = \hbar g_0 (\alpha_p + \alpha_p^*) \left[\sum_{i=1}^4 (\hat{a}_i + \hat{a}_i^\dagger) \right]^2, \quad (11)$$

where α_p denotes the coherent pump amplitude. The bosonic operators $\hat{a}_i, \hat{a}_i^\dagger$ are the annihilation and creation operators of the four cavity modes, and g_0 is an effective coupling constant. Equation (11) contains various terms corresponding to different physical processes. However, we can selectively activate different processes by an appropriate choice of pump frequency. Two cavity modes of i, j get coupled together via a coherent pump if $f_p = |f_i - f_j|$, and the Hamiltonian \hat{H}_{int} will be reduced to $\hat{H}_{CC} = \hbar g'(\hat{a}_i \hat{a}_j^\dagger + \hat{a}_j \hat{a}_i^\dagger)$. The phase of the coupling rate g' can be tuned by phase locking different pump fluxes to a reference value. In other words the coupling between different modes can be designed to be real or complex, leading to reciprocal or nonreciprocal coupling, respectively.

III. BOSONIC CREUTZ LADDER

The possibility of manipulating the phase of the coupling in a lattice of transmon qubits allows one to simulate fundamental problems in high-energy physics as well as in condensed matter. For instance, quantum Hall effects, topological states, and chiral edge modes are some of the important phenomena that could be simulated in these circuits. Based on the scheme proposed in the previous section, by proper choice of the modulation frequency and on-site energies, the hopping rate between adjacent sites in a lattice can be independently

tuned to be real- or complex-valued. As an example of the various Hamiltonians that can be simulated via this scheme, in this section we focus on a particular model that appears in multidisciplinary physics: the bosonic Creutz ladder [29–31]. This model describes a cross-linked lattice in a classical magnetic field. Due to its structure and interference effects and depending on the values of the hopping and the magnetic field, isolated edge states can appear. In fact, there is a deep connection between the domain-wall approach of the chiral modes in lattice gauge theory, and the robust nature of these states under small variations of the bond strengths; this feature is linked to the topological properties of the ladder.

In a two-leg ladder shown in Fig. 1(b) this model is described with the following Hamiltonian:

$$H = - \sum_n \left[t_d (b_n^\dagger a_{n+1} + a_n^\dagger b_{n+1}) + e^{i\phi} (a_{n+1}^\dagger a_n + b_n^\dagger b_{n+1}) + \frac{t_v}{2} (b_n^\dagger a_n + a_{n+1}^\dagger b_{n+1}) + \text{H.c.} \right]. \quad (12)$$

As depicted in Fig. 1(b), a_n and b_n are the bosonic degrees of freedom in a two-leg ladder with t_d and t_v being the hopping terms in the diagonal and vertical directions, respectively. ϕ is the magnetic flux leading to a coupling between the sites as $e^{i\phi}$, horizontally. In the Fourier basis the Hamiltonian of an N -site ladder could be written as

$$H = \sum_k \begin{pmatrix} a_k^\dagger & b_k^\dagger \end{pmatrix} \begin{pmatrix} -2 \cos\left(\frac{2\pi k}{N} + \phi\right) & -2t_d \cos\left(\frac{2\pi k}{N}\right) - t_v \\ -2t_d \cos\left(\frac{2\pi k}{N}\right) - t_v & -2 \cos\left(\frac{2\pi k}{N} - \phi\right) \end{pmatrix} \begin{pmatrix} a_k \\ b_k \end{pmatrix} = \sum_k \begin{pmatrix} a_k^\dagger & b_k^\dagger \end{pmatrix} \vec{n}_k \vec{\sigma} \begin{pmatrix} a_k \\ b_k \end{pmatrix}, \quad (13)$$

where $\sigma^{(\alpha)}$ is the α -Pauli matrix, $n_k^{(0)} = -2 \cos\left(\frac{2\pi k}{N}\right) \cos(\phi)$ (prefactor of the identity operator), $n_k^{(x)} = -2t_d \cos\left(\frac{2\pi k}{N}\right) - t_v$, and $n_k^{(z)} = 2 \sin\left(\frac{2\pi k}{N}\right) \sin(\phi)$.

After diagonalization, the Hamiltonian reads as follows:

$$H = \sum_k \begin{pmatrix} \eta_{+,k}^\dagger & \eta_{-,k}^\dagger \end{pmatrix} \begin{pmatrix} +\Lambda_k - 2 \cos\left(\frac{2\pi k}{N}\right) \cos(\phi) & 0 \\ 0 & -\Lambda_k - 2 \cos\left(\frac{2\pi k}{N}\right) \cos(\phi) \end{pmatrix} \begin{pmatrix} \eta_{+,k} \\ \eta_{-,k} \end{pmatrix}, \quad (14)$$

where $\Lambda_k = \{4 \sin^2\left(\frac{2\pi k}{N}\right) \sin^2(\phi) + [2t_d \cos\left(\frac{2\pi k}{N}\right) + t_v]^2\}^{1/2}$ and $\eta_{\pm,k}$ are linear combinations of a_k, b_k .

Depending on the parameter values in the Hamiltonian the system acquires different symmetries. We define $h_k = \vec{n}_k \vec{\sigma}$. From the Fourier description of Eq. (13), it is clear that $\sigma^x h_k \sigma^x = h_{-k}$, corresponding to the time-reversal symmetry for any parameter values of the Hamiltonian.

At $\phi = \frac{\pi}{2}$, one can obtain two additional symmetries as $\sigma^z h_k \sigma^z = -h_{-k}$ and $\sigma^y h_k \sigma^y = -h_k$, corresponding to the particle-hole symmetry and chiral symmetry, respectively. More information about the properties of the Hamiltonian and the implications of the chiral symmetry can be found in Appendix C.

At this value of the flux and in the “strong” coupling limit where the vertical coupling vanishes, $t_v = 0$, and the diagonal coupling $t_d = 1$, the Hamiltonian will be simplified as

$$H = - \sum_n (b_n^\dagger a_{n+1} + a_n^\dagger b_{n+1} + a_{n+1}^\dagger b_n + b_{n+1}^\dagger a_n) - i \sum_n (a_n^\dagger a_{n+1} + b_{n+1}^\dagger b_n - a_{n+1}^\dagger a_n - b_n^\dagger b_{n+1}) \\ = \sum_k \begin{pmatrix} a_k^\dagger & b_k^\dagger \end{pmatrix} \begin{pmatrix} 2 \sin\left(\frac{2\pi k}{N}\right) & -2 \cos\left(\frac{2\pi k}{N}\right) \\ -2 \cos\left(\frac{2\pi k}{N}\right) & -2 \sin\left(\frac{2\pi k}{N}\right) \end{pmatrix} \begin{pmatrix} a_k \\ b_k \end{pmatrix} = \sum_k \begin{pmatrix} \eta_{+,k}^\dagger & \eta_{-,k}^\dagger \end{pmatrix} \begin{pmatrix} 2 & 0 \\ 0 & -2 \end{pmatrix} \begin{pmatrix} \eta_{+,k} \\ \eta_{-,k} \end{pmatrix}, \quad (15)$$

where the “Bloch” basis $\eta_{\pm,k}$ is defined as

$$\begin{pmatrix} \eta_{+,k} \\ \eta_{-,k} \end{pmatrix} = \begin{pmatrix} \cos\left(\frac{\pi k}{N} - \frac{\pi}{4}\right) & \sin\left(\frac{\pi k}{N} - \frac{\pi}{4}\right) \\ \sin\left(\frac{\pi k}{N} - \frac{\pi}{4}\right) & -\cos\left(\frac{\pi k}{N} - \frac{\pi}{4}\right) \end{pmatrix} \begin{pmatrix} a_k \\ b_k \end{pmatrix}. \quad (16)$$

As elaborated in Appendix C in the limit of no coupling between the first and last site of the lattice the chiral modes have a simplified version given by the left and right modes as shown in Eq. (C4). To investigate the evolution of these states and the implication of the chiral edge symmetry on the particle

transport in the next part we focus on just one building block of this lattice, i.e., a four-site plaquette.

A. Four-site plaquette

Based on what is described in Appendix C, the Hamiltonian of the Creutz ladder at strong coupling when $\phi = \frac{\pi}{2}$, $t_v = 0$, and $t_d = 1$ and with the definitions of $a_n = a_1$, $a_{n+1} = a_2$, $b_n = a_3$ and $b_{n+1} = a_4$ takes the following form:

$$\begin{aligned} H &= -(a_3^\dagger a_2 + a_1^\dagger a_4 + a_2^\dagger a_3 + a_4^\dagger a_1) \\ &\quad - i(a_1^\dagger a_2 - a_2^\dagger a_1 + a_4^\dagger a_3 - a_3^\dagger a_4) \\ &= 2(\eta_+^\dagger \eta_+ - \eta_-^\dagger \eta_-), \end{aligned} \quad (17)$$

Moreover, from Eq. (C1) the Bloch states are determined as

$$\begin{aligned} \eta_+ &= \frac{1}{2}[e^{-i\pi/4}(a_2 - a_3) + e^{i\pi/4}(a_1 - a_4)], \\ \eta_- &= \frac{1}{2}[e^{i\pi/4}(a_2 + a_3) + e^{-i\pi/4}(a_1 + a_4)], \end{aligned} \quad (18)$$

where the zero modes are obtained from Eq. (C4) as

$$\begin{aligned} \eta_{0,L} &= \frac{1}{\sqrt{2}}(e^{i\pi/4}a_1 + e^{-i\pi/4}a_3), \\ \eta_{0,R} &= \frac{1}{\sqrt{2}}(e^{-i\pi/4}a_2 + e^{i\pi/4}a_4). \end{aligned} \quad (19)$$

Having the eigenstates of the Hamiltonian, it is straightforward to study the evolution of the single-particle state as below:

$$\begin{aligned} |+\rangle &= \eta_+^\dagger |0\rangle, \quad |-\rangle = \eta_-^\dagger |0\rangle, \quad |L\rangle = \eta_{0,L}^\dagger |0\rangle, \\ |R\rangle &= \eta_{0,R}^\dagger |0\rangle, \quad |+(t)\rangle = e^{-i2t}|+\rangle, \quad |-(t)\rangle = e^{i2t}|-\rangle, \\ |L(t)\rangle &= |L\rangle, \quad |R(t)\rangle = |R\rangle. \end{aligned} \quad (20)$$

Note that the second line is based on the fact that $|+\rangle$ and $|-\rangle$ have the energies of $+2$ and -2 , respectively, and $|L\rangle$ and $|R\rangle$ are the zero-energy states.

Let us assume that the system is initialized at one-particle state in the mode 1 as $|a_1\rangle = a_1^\dagger |0\rangle$. The creation operator reads

$$a_1^\dagger = \frac{e^{i\pi/4}}{2}\eta_+^\dagger + \frac{e^{-i\pi/4}}{2}\eta_-^\dagger + \frac{e^{i\pi/4}}{\sqrt{2}}\eta_{0,L}^\dagger. \quad (21)$$

Therefore, the single-particle state evolves as

$$\begin{aligned} |a_1(t)\rangle &= \frac{e^{i\pi/4}}{2}e^{-i2t}|+\rangle + \frac{e^{-i\pi/4}}{2}e^{i2t}|-\rangle + \frac{e^{i\pi/4}}{\sqrt{2}}|1\rangle \\ &= \frac{1}{2}\{[1 + \cos(2t)]|a_1\rangle + i[1 - \cos(2t)]|a_3\rangle \\ &\quad + \sin(2t)(|a_2 + i|a_4\rangle)\}. \end{aligned} \quad (22)$$

As can be seen, the behavior of the occupations of the four modes has a clear signature of chirality. Starting from the single-particle state $|a_1\rangle$ at initial time, the population of this state decreases and gets transferred to the state of $|a_2\rangle + i|a_4\rangle$. Finally, the whole population appears in $|a_3\rangle$. Figure 3 shows the population of these modes as a function of time where a clockwise transport is clear. In other words, the time evolution of the population has some direction (clockwise in this case)

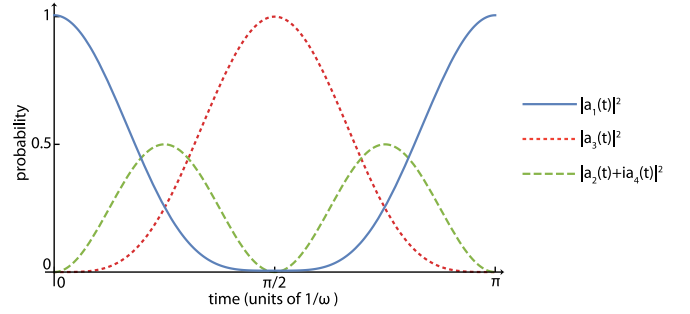


FIG. 3. Temporal dependence of the local occupations of the modes involved in a plaquette configuration. This behavior has the signature of chirality. Starting with an initial state $|a_1\rangle$, the population of this state decreases while increases $|a_2\rangle + i|a_4\rangle$ population and finally the whole population appears in $|a_3\rangle$.

which leads to complete population transfer from $|a_1\rangle$ to $|a_3\rangle$, deterministically.

As experimentally it is easier to initiate the system in a coherent state rather than a number state it is worth investigating the behavior of the system when initiated in such a coherent state. Assume that the system starts from the coherent state of the first mode in $|\alpha_{1n}\rangle$ satisfying $a_{1n}|\alpha_{1n}\rangle = \alpha_{1n}|\alpha_{1n}\rangle$. Given $|\alpha_1(t=0)\rangle = e^{-1/2}e^{a_1^\dagger}|0\rangle$ and the decomposition in terms of eigenmodes a_1^\dagger as in Eq. (21) we get

$$\begin{aligned} |\alpha_1(t)\rangle &= e^{-1/2} \exp\left(\frac{1 + \cos(2t)}{2}a_1^\dagger\right) \exp\left(\frac{\sin(2t)}{2}a_2^\dagger\right) \\ &\quad \times \exp\left(i\frac{1 - \cos(2t)}{2}a_3^\dagger\right) \exp\left(i\frac{\sin(2t)}{2}a_4^\dagger\right)|0\rangle. \end{aligned} \quad (23)$$

As can be seen, the intensity of the coherent states, i.e., $|\alpha_i(t)|^2$ follows identically the same time evolution as the one given by the single-particle state derived in Eq. (22). This results indicate that the time evolution of both Fock state as well as the coherent state in a four-site plaquette of a bosonic Creutz ladder show a similar temporal behavior.

B. Loss and interaction effect

One of the major sources of discrepancy between our model and the real cavity is loss. In reality, the photons in a cavity have a finite lifetime which leads to a loss for all the modes. Assuming the same loss κ for all the nodes, the dynamics of the open system can be approximated with a Hamiltonian as:

$$\begin{aligned} H &= - \sum_n (b_n^\dagger a_{n+1} + a_n^\dagger b_{n+1} + a_{n+1}^\dagger b_n + b_{n+1}^\dagger a_n) \\ &\quad - i(a_n^\dagger a_{n+1} + b_{n+1}^\dagger b_n - a_{n+1}^\dagger a_n - b_n^\dagger b_{n+1}) \\ &\quad - i\frac{\kappa}{2}a_n^\dagger a_n + b_n^\dagger b_n. \end{aligned} \quad (24)$$

Following the same procedure as for the conservative case and treating the system in the Fourier basis it is straightforward to show that the frequencies of the $H_{k\pm}$ are modified as $\pm 2 - i\kappa/2$. Therefore, the Hamiltonian of a four-site

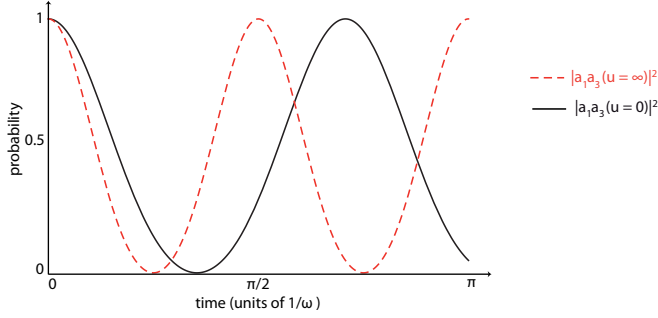


FIG. 4. Time evolution of two bosonic excitations in a Creutz plaquette. The two limiting cases (no interaction $U = 0$, and hard-core boson $U \rightarrow \infty$) can be characterized by a shift in the frequency of the time-dependent probability of finding the two excitations in the same place at a later time t .

plaquette will be modified as

$$H_l = \left(2 - i\frac{\kappa}{2}\right)\eta_+^\dagger\eta_+ + \left(2 - i\frac{\kappa}{2}\right)\eta_-^\dagger\eta_-. \quad (25)$$

This means for a system initiated at one-particle state of $|a_1\rangle$, the time evolution of Eq. (22) follows the modified form of

$$|a_1(t)\rangle = \frac{e^{i\pi/4}}{2}e^{-i(2-i\kappa/2)t}|+\rangle + \frac{e^{-i\pi/4}}{2}e^{-i(2-i\kappa/2)t}|-\rangle + \frac{e^{i\pi/4}}{\sqrt{2}}e^{-\kappa/2t}|1\rangle = |a_1(t)\rangle_{\text{lossless}}e^{-\kappa/2t}. \quad (26)$$

The last equation simply implies that modes of a lossy plaquette have the same dynamics as a closed system with an additional general loss due to the finite lifetime of the photons in a real cavity. Therefore, the edge mode is still present in the system and the chiral transport of the particle from the first to the third node can still be observed if $\kappa\pi \leq 4$.

One of the main features of implementing complex hopping terms, in a setup built out of transmons is the possibility to modify the on-site energies of the local degrees of freedom. This fact allows us to enter in phases of interacting quantum many-body systems in the presence of a magnetic field such as the fractional quantum Hall effect. As a final analysis, we show that the on-site energy already changes the dynamics of a Creutz plaquette, noticeably. For this purpose, we study the dynamics of two bosonic excitations in the plaquette in two relevant limits, when there is no on-site interaction in the bosonic field, i.e., a free bosonic field ($U = 0$), and where the on-site interaction is so strong that the system is described by a hard-core boson limit, i.e., only the empty and single-occupied state are allowed, so we can characterize the local Hilbert space by a two-level system ($U \rightarrow \infty$).

As a case of study, we investigate the two-particle dynamics in the plaquette, loading the system with two excitations in the first and third sites, i.e., $|\psi(t=0)\rangle = \hat{a}_1^\dagger\hat{a}_3^\dagger|0\rangle = |1_1, 1_3\rangle$ and compute the probability of finding them in the first and third sites at a later time t . In the non-interacting limit, we get an analytic expression for this probability, $|\langle 1_1, 1_3|1_1, 1_3(t)\rangle|^2 = [\cos^4(t) + \sin^4(t)]^2$, that can be compared with the interacting case where the shift in the frequency signals the non-trivial interactions between the particles (see

Fig. 4). This shift and the interpolation between both limits can be measured with modern quantum technologies in a circuit QED platform. This indicates the presence or absence of interaction in a plaquette and can be scaled up to a whole ladder or even to a two-dimensional (2D) lattice.

IV. CONCLUSION

In this work we propose a method based on modulating the on-site flux of coupled transmons in a lattice to induce a non-zero phase for the coupling term between adjacent sites. The phase of the coupling can be broadly tuned as a function of the modulation frequency, modulation depth, and site energies. The possibility of having arbitrary complex-valued couplings opens a door to simulating several important models.

As an example, we chose the bosonic Creutz ladder as an important Hamiltonian arising in several disciplines ranging from high-energy physics to condensed matter. The important ingredients of this Hamiltonian, the complex-valued couplings, can be realized based on the proposed scheme. Several interesting features arise in such a lattice, including topological and chiral edge modes. To investigate the behavior we focused our study and numerical modeling on one plaquette of the lattice, i.e., a four-site building block. As shown by our calculations chiral edge modes appear in this configuration where a directional population transfer along the plaquette edges can be observed for both the single-particle as well as the coherent states. Moreover, we propose an experimental scheme based on parametric coupling between cavity modes. By controlling the phase and frequency of the pump, one can engineer the Hamiltonian of a four-site Creutz ladder. This experimental proposal is readily achievable with state-of-the-art circuit QED technology. To measure the directional transfer, one measures the intermodal scattering when the cavity is excited at one mode and power is detected at another. By measuring the asymmetry of the scattering parameters, say the transmission from node 1 to 2 versus node 2 to 1, the directional transfer can be inferred. This technique is, for instance, clearly demonstrated in Ref. [28].

The method presented in this paper is extendable and applicable for 2D lattices where the hopping term between adjacent lattice sites can be easily manipulated. Moreover, by employing the inherent nonlinearity of the transmon Hamiltonian, the proposal can be extended even further to include on-site interactions as well. By changing the ratio of the on-site interaction energy U , and the coupling J , the behavior of a lattice in phase space can span all the way from a Mott insulator (for large ratio) to the superfluid phase (for small ratio). The proposed method combined with the existing circuit QED technology makes these systems one of the most promising and versatile candidates for simulating rich physics from condensed-matter systems to high-energy problems.

ACKNOWLEDGMENTS

H.A. acknowledges the financial support from Alexander von Humboldt foundation in terms of a postdoctoral fellowship. E.R. and E.S. acknowledge funding from MINECO/FEDER FIS2015-69983-P and the Basque

Government IT986-16. This material is also based on work supported by the projects OpenSuperQ and QMiCS of the EU Flagship on Quantum Technologies. E.R. also acknowledges EU support from the QuantERA program under the QTFlag project. C.M.W., C.W.S.C., and M.V.M. acknowledge NSERC of Canada, the Canadian Foundation for Innovation, the Ontario Ministry of Research and Innovation, Canada First Research Excellence Fund (CFREF), Industry Canada, and the CMC for financial support.

APPENDIX A: TRANSMON QUBIT

A transmon is one of the basic elements of the circuit QED consisting of a capacitor in parallel with a Josephson junction [13,32,33]. Due to the inherent nonlinearity of the latter element, the harmonicity of an LC-circuit oscillator is removed and an effective two-level atom is obtained. The following expression gives the Hamiltonian of a transmon, which consists of a capacitor C and a Josephson junction with energy E_J :

$$\hat{\mathcal{H}}_{\text{NLC}} = \frac{\hat{Q}^2}{2C} - E_J \cos\left(\frac{\hat{\phi}}{\phi_0}\right), \quad (\text{A1})$$

where \hat{Q} and $\hat{\phi}$ are charge and flux operators satisfying the canonical commutation relation of $[\hat{\phi}, \hat{Q}] = i\hbar$.

For small flux we can Taylor expand the nonlinear term $\cos(\hat{\phi}/\phi_0)$ around zero and rewrite the Hamiltonian in the form of $\hat{\mathcal{H}}_{\text{NLC}} = \hat{\mathcal{H}}_0 + \hat{\mathcal{H}}_1$ as follows:

$$\hat{\mathcal{H}}_0 = \frac{\hat{Q}^2}{2C} + \frac{E_J}{\phi_0^2} \frac{\hat{\phi}^2}{2} = \frac{\hat{Q}^2}{2C} + \frac{\hat{\phi}^2}{2L}, \quad (\text{A2a})$$

$$\hat{\mathcal{H}}_1 = -E_J \left[\cos\left(\frac{\hat{\phi}}{\phi_0}\right) - 1 + \frac{\hat{\phi}^2}{2\phi_0^2} \right]. \quad (\text{A2b})$$

In the above equations $\hat{\mathcal{H}}_0$ is the Hamiltonian of a harmonic oscillator with capacitance C and an effective inductance $L = \phi_0^2/E_J$. The remaining operator $\hat{\mathcal{H}}_1$ is the nonlinear part of the Hamiltonian.

We define the normalized, dimensionless charge \hat{q} and flux $\hat{\phi}$ as

$$\hat{q} = \frac{\hat{Q}}{\sqrt{\hbar^2 C/L}}, \quad \hat{\phi} = \frac{\hat{\phi}}{\sqrt{\hbar^2 L/C}}. \quad (\text{A3})$$

Substituting these normalized variables in the harmonic oscillator Hamiltonian, the linear part $\hat{\mathcal{H}}_0$ could be rewritten as the canonical form of a quantum harmonic oscillator as

$$\hat{\mathcal{H}}_0 = \frac{\hbar\omega_0}{2} (\hat{q}^2 + \hat{\phi}^2) = \hbar\omega_0 \left(\hat{a}^\dagger \hat{a} + \frac{1}{2} \right), \quad (\text{A4})$$

where $\omega_0 = \sqrt{1/LC}$ is the resonance frequency of the linear LC circuit, and the bosonic operators \hat{a} and \hat{a}^\dagger are the annihilation and creation operators defined as $\hat{\phi} = (\hat{a} + \hat{a}^\dagger)/\sqrt{2}$ and $\hat{q} = i(\hat{a}^\dagger - \hat{a})/\sqrt{2}$.

Although in this paper we do not require the nonlinear behavior of the Josephson junction, for sake of completeness we briefly derive various interaction terms that can be obtained with a transmon qubit.

In a typical transmon qubit the Josephson junction energy exceeds the capacitor energy, i.e., $E_J \gg E_C$. Therefore,

$\epsilon = \sqrt{8E_C/E_J} \ll 1$, and one can express $\cos(\hat{\phi}/\phi_0)$ in terms of normal ordered operator products as

$$\cos\left(\sqrt{\frac{\epsilon}{2}}(\hat{a} + \hat{a}^\dagger)\right) = e^{-\frac{\epsilon}{4}} \sum_{n,m;n+m=\text{even}} \frac{\left(-\frac{\epsilon}{2}\right)^{\frac{n+m}{2}}}{n!m!} (\hat{a}^\dagger)^n \hat{a}^m. \quad (\text{A5})$$

Keeping the number-conserving operators only, the nonlinear part of Hamiltonian takes the following form:

$$\hat{\mathcal{H}}_1 \simeq \hbar\delta\omega_0 \hat{a}^\dagger \hat{a} - \hbar\Omega \hat{a}^\dagger \hat{a}^\dagger \hat{a} \hat{a} + \frac{\hbar\Omega'}{6} \hat{a}^\dagger \hat{a}^\dagger \hat{a}^\dagger \hat{a} \hat{a} \hat{a} + \dots \quad (\text{A6})$$

In this last equation the frequency shift and interaction energies are given by

$$\delta\omega_0 = \sqrt{2E_J E_C} (1 - e^{-\frac{\epsilon}{4}}), \quad \Omega = \frac{E_C}{2} e^{-\frac{\epsilon}{4}}, \quad \Omega' = \frac{\epsilon}{3} \Omega. \quad (\text{A7})$$

The harmonic frequency shift can be absorbed into a redefinition of ω_0 , i.e., $\omega_0 + \delta\omega_0 - \Omega \rightarrow \omega_0$, and for low excitation numbers the transmon Hamiltonian would be simplified as

$$\hat{\mathcal{H}}_{T_r} \simeq \hbar\omega_0 \hat{a}^\dagger \hat{a} - \hbar\Omega (\hat{a}^\dagger \hat{a})^2. \quad (\text{A8})$$

APPENDIX B: COUPLED TRANSMONS

Consider a circuit of two transmons coupled together via a capacitor C_J and an inductor L_J as shown in Fig. 1(a). To distinguish the variables, we use (ϕ_l, q_l) and (ϕ_r, q_r) for the flux and charge of the left and right transmons, respectively. The Lagrangian of the full circuit is given by

$$\mathcal{L} = \left[\frac{C_l}{2} \dot{\phi}_l^2 + E_{Jl} \cos\left(\frac{\phi_l}{\phi_0}\right) \right] + \left[\frac{C_r}{2} \dot{\phi}_r^2 + E_{Jr} \cos\left(\frac{\phi_r}{\phi_0}\right) \right] + \frac{C_J}{2} (\dot{\phi}_r - \dot{\phi}_l)^2 - \frac{1}{2L_J} (\phi_r - \phi_l)^2, \quad (\text{B1})$$

where C_η and $E_{J\eta}$ denote the capacitance and Josephson-junction energy of each subcircuit, $\eta = l, r$, and L_J and C_J are the inductance and capacitance of the coupling branch. We introduce the node charges $Q_\eta = \frac{\partial \mathcal{L}}{\partial \phi_\eta}$ fulfilling commutation relations $[\hat{\phi}_\eta, \hat{Q}_{\eta'}] = i\hbar\delta_{\eta,\eta'}$. By introducing a vector notation $\hat{\phi} \equiv (\hat{\phi}_l, \hat{\phi}_r)$ and $\hat{Q} \equiv (\hat{Q}_l, \hat{Q}_r)$, the equivalent Hamiltonian can be written as

$$\hat{\mathcal{H}} = \frac{1}{2} \hat{Q} C^{-1} \hat{Q}^T - \left[E_{Jl} \cos\left(\frac{\hat{\phi}_l}{\phi_0}\right) + E_{Jr} \cos\left(\frac{\hat{\phi}_r}{\phi_0}\right) \right] + \frac{1}{2L_J} (\hat{\phi}_r - \hat{\phi}_l)^2, \quad (\text{B2})$$

where C is the capacitance matrix given by the following equation:

$$C = \begin{pmatrix} C_l + C_J & -C_J \\ -C_J & C_r + C_J \end{pmatrix}. \quad (\text{B3})$$

Equation (B2) can be further simplified to get the following Hamiltonian for the two coupled transmons:

$$\hat{\mathcal{H}} = \left[\frac{1}{2} \frac{C_r + C_J}{C_r C_l + C_r C_J + C_l C_J} \hat{Q}_l^2 - E_{Jl} \cos\left(\frac{\hat{\phi}_l}{\phi_0}\right) + \frac{1}{2L_J} \hat{\phi}_l^2 \right] + \left[\frac{1}{2} \frac{C_l + C_J}{C_r C_l + C_r C_J + C_l C_J} \hat{Q}_r^2 - E_{Jr} \cos\left(\frac{\hat{\phi}_r}{\phi_0}\right) + \frac{1}{2L_J} \hat{\phi}_r^2 \right] + \frac{C_J}{C_r C_l + C_r C_J + C_l C_J} \hat{Q}_r \hat{Q}_l - \frac{1}{L_J} \hat{\phi}_r \hat{\phi}_l. \quad (\text{B4})$$

Without inductive coupling, the first two terms in each bracket are Hamiltonians of two transmons with modified shunt capacitors, and the last term describes the interaction Hamiltonian via capacitive coupling. As can be seen, both of the capacitive and inductive couplings have the same form and only the sign of the interaction is different. Therefore, without loss of generality one can consider one type of coupling only, and the results are properly applicable to the other type via duality. In what follows we focus on the inductive case, i.e., $C_J = 0$.

The presence of the coupling inductance L_J modifies the effective inductance of each transmon, so the new natural frequency of each qubit is given as

$$\omega_{0_{l/r}} = \sqrt{\frac{1}{C_{l/r}} \left(\frac{1}{L_J} + \frac{E_{J_{l/r}}}{\phi_0^2} \right)} = \frac{1}{\sqrt{C_{l/r} L_{l/r}^*}}. \quad (\text{B5})$$

By using the normalized variables as in Eq. (A3) and their corresponding bosonic operators, the coupled qubits dynamics is determined via the following Hamiltonian:

$$\hat{\mathcal{H}} = \hbar\omega_{0l} \left(\hat{a}_l^\dagger \hat{a}_l + \frac{1}{2} \right) + \hbar\omega_{0r} \left(\hat{a}_r^\dagger \hat{a}_r + \frac{1}{2} \right) - \frac{\hbar}{2} \sqrt{\frac{L_l^* L_r^*}{L_J^2}} \sqrt{\omega_{0l} \omega_{0r}} (\hat{a}_r \hat{a}_l^\dagger + \hat{a}_r^\dagger \hat{a}_l). \quad (\text{B6})$$

Notice that, in the last parentheses, we dropped the non-particle-conserving terms of $\hat{a}_r \hat{a}_l + \hat{a}_r^\dagger \hat{a}_l^\dagger$, which is a valid assumption in the rotating wave approximation (RWA) limit. This final equation corresponds to the Hamiltonian of two harmonic oscillators on the left and right (i.e., the first-order approximation of the qubit) while the last term describes the hopping between those qubits.

Now assume that the Josephson junction energy of each transmon is harmonically modulated as $E_{J_{l,r}}(t) = E_{J_{l,r}}^0 + e_{J_{l,r}} \cos(\omega_M t + \Phi_{0_{l,r}})$. Plugging this form back into Eq. (B6) and assuming a weak modulation, i.e., $e_{J_{l,r}} \ll E_{J_{l,r}}^0$, the Hamiltonian of the two-coupled qubits would be modified as

$$\hat{\mathcal{H}} = \hbar\omega_{0l} \left(1 + \frac{1}{2} \frac{e_{Jl} L_J}{\phi_0^2 + E_{Jl}^0 L_J} \cos(\omega_M t + \Phi_{0l}) \right) \left(\hat{a}_l^\dagger \hat{a}_l + \frac{1}{2} \right) + \hbar\omega_{0r} \left(1 + \frac{1}{2} \frac{e_{Jr} L_J}{\phi_0^2 + E_{Jr}^0 L_J} \cos(\omega_M t + \Phi_{0r}) \right) \left(\hat{a}_r^\dagger \hat{a}_r + \frac{1}{2} \right) - \frac{\hbar}{2} \sqrt{\frac{L_l^* L_r^*}{L_J^2}} \sqrt{\omega_{0l} \omega_{0r}} (\hat{a}_l \hat{a}_r^\dagger + \hat{a}_r \hat{a}_l^\dagger). \quad (\text{B7})$$

Since the modulation has a second-order effect on the coupling term, those corrections have been ignored in the first-order calculation which is the main scope of this paper.

APPENDIX C: BOSONIC CREUTZ LADDER

The chiral symmetry of the Creutz ladder is briefly discussed in the main text. In this Appendix these features will be elaborated in more detail.

As discussed in the main text at $\phi = \frac{\pi}{2}$, the Hamiltonian possesses the chiral symmetry as $\sigma^y h_k \sigma^y = -h_k$, for all k within the first Brillouin zone. The chiral symmetry implies that any eigenstate $|E\rangle$ with energy E has a counterpart $| -E\rangle = \sigma^y |E\rangle$ with energy $-E$. Therefore, in a chiral-symmetric system, the eigenstates come in pairs at $\pm E$.

For a state at $E = 0$, the state is its own partner, i.e., $|E = 0\rangle = \sigma^y |E = 0\rangle$.

To explicitly construct this zero mode, we use the low-energy continuum theory. We consider the limit $|t_v| < |t_d| < 1$ and focus on the low-energy states near $\frac{2\pi k}{N\alpha} = \frac{\pi}{\alpha} + q$,

with lattice spacing α and small q . In real space $q \rightarrow -i\partial_x$ and $H \rightarrow -iv_F \sigma^z \partial_x + m\sigma^x$, with $v_F = 2\alpha$ and $m = 2t_d - t_v$. To describe the zero mode we allow $m(x)$ to vary spatially with a kink such that $m(x \rightarrow +\infty) > 0$ and $m(x \rightarrow -\infty) < 0$. A zero-energy solution $H|E = 0\rangle = 0$ can be constructed by considering eigenstates $|\pm y\rangle$ of σ^y with eigenvalue ± 1 , giving $\partial_x \psi_{0,\pm}(x) = \pm \frac{m(x)}{v_F} \psi_{0,\pm}(x)$. Integrating the first-order equation leads to a single normalizable solution as $\psi_{0,-}(x) = e^{-\int_0^x dx' \frac{m(x')}{v_F}}$. This solution is a localized wave function at $x = 0$ with exponentially decaying tails on the sides.

Due to the periodicity of the Hamiltonian in k , all integers k within $(-N/2, +N/2]$ define a closed curve in the $(n_k^{(x)} - n_k^{(z)})$ plane whose features strongly depend on the ratio $\mathcal{R} = t_v/t_d$. If $|\mathcal{R}| < 2$, this curve will enclose the origin (0,0) where the Hamiltonian is strictly zero. On the other hand, if $|\mathcal{R}| > 2$ the curve will not enclose this point and is deformed to a trivial one. When $|\mathcal{R}| < 2$, the number of times the closed curve winds around the origin defines a topological invariant called the *winding number* ν .

The Bloch states of the periodic lattice is defined in Eq. (16) of the main text in Fourier space. To find the maximally localized “Wannier” basis, which basically is the Bloch states representation in real space, we can employ the Fourier transform as

$$\begin{aligned} \begin{pmatrix} \eta_{+,n+1/2} \\ \eta_{-,n+1/2} \end{pmatrix} &= \frac{1}{\sqrt{N}} \sum_k e^{i2\pi k(n+1/2)/N} \begin{pmatrix} \cos(\frac{\pi k}{N} - \frac{\pi}{4}) & \sin(\frac{\pi k}{N} - \frac{\pi}{4}) \\ \sin(\frac{\pi k}{N} - \frac{\pi}{4}) & -\cos(\frac{\pi k}{N} - \frac{\pi}{4}) \end{pmatrix} \begin{pmatrix} a_k \\ b_k \end{pmatrix} \\ &= \frac{1}{2} \begin{pmatrix} e^{-i\pi/4}(a_{n+1} - b_n) + e^{i\pi/4}(a_n - b_{n+1}) \\ -e^{i\pi/4}(a_{n+1} + b_n) - e^{-i\pi/4}(a_n + b_{n+1}) \end{pmatrix}. \end{aligned} \quad (C1)$$

One can show that the center of the maximally localized Wannier function gives the Berry phase of the band [34]. For the lower energy mode we have

$$|\eta_{-,n+1/2}\rangle = \frac{1}{\sqrt{N}} \sum_k e^{i2\pi k(n+1/2)/N} |\eta_{-,k}\rangle, \quad \langle \eta_{-,n+1/2} | \hat{m} | \eta_{-,n+1/2} \rangle = -\frac{i}{2\pi} \sum_k \langle \eta_{-,k} | \frac{\partial}{\partial k} | \eta_{-,k} \rangle = \frac{\phi_{\text{Berry}}}{2\pi}, \quad (C2)$$

where \hat{m} is the position operator in the discrete space of the lattice.

Moreover, the expectation value of the position of the Wannier functions can be found by using Eq. (C1), giving the relation between the Wannier and the lattice operators we have

$$\begin{aligned} \langle \eta_{-,n+1/2} | \hat{m} | \eta_{-,n+1/2} \rangle &= [e^{-i\pi/4}(\langle a_{n+1} | + \langle b_n |) + e^{i\pi/4}(\langle a_n | + \langle b_{n+1} |)] \frac{\hat{m}}{4} [e^{i\pi/4}(|a_{n+1}\rangle + |b_n\rangle) + e^{-i\pi/4}(|a_n\rangle + |b_{n+1}\rangle)] \\ &= \frac{1}{4} [\langle a_{n+1} | (n+1) | a_{n+1} \rangle + \langle b_n | n | b_n \rangle + \langle a_n | n | a_n \rangle + \langle b_{n+1} | (n+1) | b_{n+1} \rangle] = n + \frac{1}{2}. \end{aligned} \quad (C3)$$

Therefore, the Berry phase of the lower band in the Creutz ladder is $\phi_{\text{Berry}} - 2\pi n = \pi$.

From the definition of the Wannier operators in terms of the original operators we can see that, in the absence of the coupling between the first and the last site of the ladder, there are two zero modes described via the following relations:

$$\eta_{0,L} = \frac{1}{\sqrt{2}}(e^{i\pi/4} a_1 + e^{-i\pi/4} b_1), \quad \eta_{0,R} = \frac{1}{\sqrt{2}}(e^{-i\pi/4} a_N + e^{i\pi/4} b_N). \quad (C4)$$

While $\eta_{0,L}$ is only dependent on the left side of the ladder, $\eta_{0,R}$ only depends on the right-most branch.

-
- [1] M. Devoret, B. Huard, R. Schoelkopf, and L. F. Cugliandolo, *Quantum Machines: Measurement and Control of Engineered Quantum Systems*, Lecture Notes of the Les Houches Summer School (Oxford University Press, Oxford, UK, 2011), Vol. 96.
- [2] J. Koch, A. A. Houck, K. L. Hur, and S. M. Girvin, Time-reversal-symmetry breaking in circuit-QED-based photon lattices, *Phys. Rev. A* **82**, 043811 (2010).
- [3] A. Nunnenkamp, J. Koch, and S. Girvin, Synthetic gauge fields and homodyne transmission in Jaynes–Cummings lattices, *New J. Phys.* **13**, 095008 (2011).
- [4] A. A. Houck, H. E. Türeci, and J. Koch, On-chip quantum simulation with superconducting circuits, *Nat. Phys.* **8**, 292 (2012).
- [5] S. Schmidt and J. Koch, Circuit QED lattices: Towards quantum simulation with superconducting circuits, *Ann. Phys. (Berlin, Ger.)* **525**, 395 (2013).
- [6] E. Kapit, Quantum simulation architecture for lattice bosons in arbitrary, tunable, external gauge fields, *Phys. Rev. A* **87**, 062336 (2013).
- [7] R. Barends, A. Shabani, L. Lamata, J. Kelly, A. Mezzacapo, U. L. Heras, R. Babbush, A. G. Fowler, B. Campbell, Y. Chen, Z. Chen, B. Chiaro, A. Dunsworth, E. Jeffrey, E. Lucero, A. Megrant, J. Y. Mutus, M. Neeley, C. Neill, P. J. J. O’Malley, C. Quintana, P. Roushan, D. Sank, A. Vainsencher, J. Wenner, T. C. White, E. Solano, H. Neven, and J. M. Martinis, Digitized adiabatic quantum computing with a superconducting circuit, *Nature (London)* **534**, 222 (2016).
- [8] P. Roushan, C. Neill, A. Megrant, Y. Chen, R. Babbush, R. Barends, B. Campbell, Z. Chen, B. Chiaro, A. Dunsworth, A. Fowler, E. Jeffrey, J. Kelly, E. Lucero, J. Mutus, P. J. J. O’Malley, M. Neeley, C. Quintana, D. Sank, A. Vainsencher, J. Wenner, T. C. White, E. Solano, H. Neven, and J. M. Martinis, Chiral ground-state currents of interacting photons in a synthetic magnetic field, *Nat. Phys.* **13**, 146 (2016).
- [9] D. Jaksch and P. Zoller, Creation of effective magnetic fields in optical lattices: The Hofstadter butterfly for cold neutral atoms, *New J. Phys.* **5**, 56 (2003).
- [10] J. Dalibard, F. Gerbier, G. Juzeliunas, and P. Ohberg, Colloquium: Artificial gauge potentials for neutral atoms, *Rev. Mod. Phys.* **83**, 1523 (2011).
- [11] R. O. Umucalilar and I. Carusotto, Artificial gauge field for photons in coupled cavity arrays, *Phys. Rev. A* **84**, 043804 (2011).
- [12] R. O. Umucalilar and I. Carusotto, Fractional Quantum Hall States of Photons in an Array of Dissipative Coupled Cavities, *Phys. Rev. Lett.* **108**, 206809 (2012).
- [13] D. Marcos, P. Rabl, E. Rico, and P. Zoller, Superconducting Circuits for Quantum Simulation of Dynamical Gauge Fields, *Phys. Rev. Lett.* **111**, 110504 (2013).
- [14] M. Hafezi, M. D. Lukin, and J. M. Taylor, Non-equilibrium fractional quantum Hall state of light, *New J. Phys.* **15**, 063001 (2013).
- [15] Q. Lin and S. Fan, Light Guiding by Effective Gauge Field for Photons, *Phys. Rev. X* **4**, 031031 (2014).
- [16] A. Eckardt, P. Hauke, P. Soltan-Panahi, C. Becker, K. Sengstock, and M. Lewenstein, Frustrated quantum antiferromagnetism with ultracold bosons in a triangular lattice, *Europhys. Lett.* **89**, 10010 (2010).

- [17] A. R. Kolovsky, Creating artificial magnetic fields for cold atoms by photon-assisted tunneling, *Europhys. Lett.* **93**, 20003 (2011).
- [18] N. Goldman and J. Dalibard, Periodically Driven Quantum Systems: Effective Hamiltonians and Engineered Gauge Fields, *Phys. Rev. X* **4**, 031027 (2014).
- [19] O. Kyriienko and A. S. Sorensen, Floquet Quantum Simulation with Superconducting Qubits, *Phys. Rev. Appl.* **9**, 064029 (2018).
- [20] N. H. Lindner, G. Refael, and V. Galitski, Floquet topological insulator in semiconductor quantum wells, *Nat. Phys.* **7**, 490 (2011).
- [21] K. Fang, Z. Yu, and S. Fan, Realizing effective magnetic field for photons by controlling the phase of dynamic modulation, *Nat. Photonics* **6**, 782 (2012).
- [22] M. C. Rechtsman, J. M. Zeuner, Y. Plotnik, Y. Lumer, D. Podolsky, F. Dreisow, S. Nolte, M. Segev, and A. Szameit, Photonic Floquet topological insulators, *Nature (London)* **496**, 196 (2013).
- [23] M. Reagor, C. B. Osborn, N. Tezak, A. Staley, G. Prawiroatmodjo, M. Scheer, N. Alidoust, E. A. Sete, N. Didier, M. P. da Silva *et al.*, Demonstration of universal parametric entangling gates on a multi-qubit lattice, *Sci. Adv.* **4**, eaao3603 (2018).
- [24] S. A. Caldwell *et al.*, Parametrically Activated Entangling Gates Using Transmon Qubits, *Phys. Rev. Appl.* **10**, 034050 (2018).
- [25] C. M. Wilson, G. Johansson, A. Pourkabirian, M. Simoen, J. R. Johansson, T. Duty, F. Nori, and P. Delsing, Observation of the dynamical Casimir effect in a superconducting circuit, *Nature (London)* **479**, 376 (2011).
- [26] E. Flurin, N. Roch, F. Mallet, M. H. Devoret, and B. Huard, Generating Entangled Microwave Radiation Over Two Transmission Lines, *Phys. Rev. Lett.* **109**, 183901 (2012).
- [27] C. W. Sandbo Chang, M. Simoen, J. Aumentado, C. Sabín, P. Forn-Díaz, A. M. Vadiraj, F. Quijandría, G. Johansson, I. Fuentes, and C. M. Wilson, Generating Multimode Entangled Microwaves with a Superconducting Parametric Cavity, *Phys. Rev. Appl.* **10**, 044019 (2018).
- [28] F. Lecocq, L. Ranzani, G. A. Peterson, K. Cicak, R. W. Simmonds, J. D. Teufel, and J. Aumentado, Nonreciprocal Microwave Signal Processing with a Field-Programmable Josephson Amplifier, *Phys. Rev. Appl.* **7**, 024028 (2017).
- [29] M. Creutz, End States, Ladder Compounds, and Domain-Wall Fermions, *Phys. Rev. Lett.* **83**, 2636 (1999).
- [30] A. Bermudez, D. Patanè, L. Amico, and M. A. Martin-Delgado, Topology-Induced Anomalous Defect Production by Crossing a Quantum Critical Point, *Phys. Rev. Lett.* **102**, 135702 (2009).
- [31] J. Jünemann, A. Piga, S.-J. Ran, M. Lewenstein, M. Rizzi, and A. Bermudez, Exploring Interacting Topological Insulators with Ultracold Atoms: The Synthetic Creutz-Hubbard Model, *Phys. Rev. X* **7**, 031057 (2017).
- [32] J. Koch, T. M. Yu, J. Gambetta, A. A. Houck, D. I. Schuster, J. Majer, A. Blais, M. H. Devoret, S. M. Girvin, and R. J. Schoelkopf, Charge-insensitive qubit design derived from the Cooper pair box, *Phys. Rev. A* **76**, 042319 (2007).
- [33] J. Clarke and F. K. Wilhelm, Superconducting quantum bits, *Nature (London)* **453**, 1031 (2008).
- [34] D. Vanderbilt, *Berry Phases in Electronic Structure Theory: Electric Polarization, Orbital Magnetization and Topological Insulators* (Cambridge University Press, Cambridge, UK, 2018).